BULLETIN OF THE EARTHQUAKE
RESEARCH INSTITUTE
Vol. 56 (1981), pp. 67-89

4. Frequency Dependence of Acoustic Emission Activity in Rocks under Incremental, Uniaxial Compression.

By Mitiyasu OHNAKA and Kiyoo MOGI,

Earthquake Research Institute.

(Received February 12, 1981)

Abstract

Acoustic emission generated during the deformation of rock under compression was monitored simultaneously through different frequency windows under a fixed condition of the monitoring channels throughout experimental runs, and the count rate of the emission events monitored through a low frequency window was compared with that of those monitored through a higher frequency window throughout the whole process from application of loading to failure. The deformation process of brittle rock under incremental compression may be commonly divided into the following five stages in terms of the emission rates. At low stresses in the region where a flurry of acoustic emission activity occurs, the activity is mostly due to low frequency acoustic emissions, presumably resulting from the closing of preexisting cracks with low aspect ratio at large angles to the compression axis (first stage). At higher stresses, the activity dies down to a very low level (second stage). As the stress is further increased gradually, again acoustic emission activity begins to build up and steadily increases (the emission rate increases exponentially with time when the applied stress rate is constant): both the emission rates $n(l)$ and $n(h)$ monitored through a low frequency window and a higher frequency window, respectively, increase with time at statistically the same proportion; that is, $n(l)/\{n(l)+n(h)\}$ is nearly constant throughout this stage (third stage). As the failure time approaches, both $n(l)$ and $n(h)$ increase supraexponentially with time, and the increase rate of $n(l)$ becomes more rapid than that of $n(h)$ until immediately before failure (fourth stage); in other words, this stage is characterized by an increase in $n(l)/\{n(l)+n(h)\}$ with time or by a higher level of $n(l)/\{n(l)+n(h)\}$. The final (fifth) stage is characterized by a very rapid acceleration of higher frequency acoustic emission activity immediately before and during failure; as a result, failure occurs immediately after $n(l)/\{n(l)+n(h)\}$ is lowered. One interesting feature in these stages is that the increase rate of the acoustic emission counted through a lower frequency window becomes more rapid with

time in the fourth stage. This is not due to the change in an applied stress level itself, but due to the change in structure within the deforming rock; the two possible explanations are given for this in this text. The beginning of the fourth stage is not concurrent with the onset of dilatancy: appreciable dilatancy always begins to occur prior to the beginning of the fourth stage. The effect in this stage is consistent with the fact that a greater number of emission events with larger amplitude increase in relative terms (namely, the decrease in m-value) as rock approaches failure, since crackings resulting in larger size tend to generate acoustic waves with both larger amplitudes and lower frequency components. Thus, it is presumable that the decrease in m-value and the frequency dependence of acoustic emission rate are different manifestations of an aspect of the fracturing process to failure. A greater number of higher frequency emission events observed in the fifth stage may be thought to be those originating around the transducers as a result of local stress concentrations near the transducers during the process of forming final macroscopic cracks. The effect found here may be used for understanding structural instability of the region where earthquakes (or rock bursts in mines) can occur potentially, and for predicting the time when a main earthquake occurs in the region, in terms of frequency contained in seismic waves if a sizable microearthquake population is observed through transducers placed near the fault.

Introduction

When rock is stressed to failure, microcracking occurs prior to macroscopic fracture, and this microcracking emits elastic radiation, which is known as acoustic emission. Microcracking in stressed rock can be detected by monitoring acoustic emission and hence acoustic emission is essentially important in understanding the fracturing process of rock. Acoustic emission, which itself is microseismic activity, is considered to be a scale model of seismicity in the Earth (MOGI, 1967). Potentially acoustic emission study can provide a physical basis for interpreting observed seismicity in the Earth and for predicting earthquakes.

Acoustic emission studies related to rocks were initiated by OBERT (1941) and OBERT and DUVALL (1942) to predict rock bursts in mines, and have been made by various authors from different viewpoints. Considerable progress has been made in this field, and several reviews have appeared on these studies (KNILL et al., 1968; HARDY, 1972 and 1977; MOGI, 1973; SHAMINA, 1975; BYERLEE, 1978). It is not clear, however, whether the spectra of acoustic waves generated during rock deformation shift toward lower or higher frequencies as rock approaches failure, though several studies (SHAMINA, 1956; CHUGH et al., 1968; KANAGAWA

et al., 1977 ; KUSUNOSE et al., 1980) have been made on this subject under incremental loading conditions. All of the earlier authors focused attention on the change in spectral amplitudes of acoustic waves over a wide-band of monitoring frequencies with increasing applied stress, and conflicting reports have been made. Some may consider that these conflicting results may be due to some difference in the experimental conditions adopted or the stress range investigated, while others may feel that the approaches taken should be called in question.

The problem whether the dominant band of acoustic wave spectra shifts to lower or higher frequencies before macroscopic fracture occurs is related to earthquake prediction studies. FEDOTOV et al. (1972) reported that the maximum spectral amplitude of seismic waves shifts to lower frequencies before a main earthquake occurs in the Kamchatka region. UTSU (1980), however, showed that "high frequency" (or normal) earthquakes occurred almost exclusively before the occurrence of major interplate earthquakes, while a considerable number of low frequency earthquakes occurred after the occurrence of major interplate earthquakes.

In the statistical analysis of the fracturing process of brittle rock, the amplitude distributions of emission events have been studied by MOGI (1962a, b and 1981), SCHOLZ (1968c) and others. A conventional way of displaying the amplitude distribution data is to use a log-log plot of the cumulative number of events versus the maximum trace amplitude. The curve is a monotonically decreasing function of the amplitude and generally can be expressed by one or more straight line segments. The slope of the curve, which is called "m-value" or "b-value" ($m=b+1$), is a manifestation of the amplitude distribution. MOGI (1962b) found that the m-value before the main fracture is lower than that after the main fracture. SCHOLZ (1968c) found that m-value decreases as rock approaches failure under incremental compressive stress, and he ascribed the decrease in m-value to the increase in the stress level. Recently, however, one of the authors performed careful experiments on amplitude distributions of acoustic emission monitored through different frequency windows under a constant stress, and confirmed the decrease in m-value before failure occurs (MOGI, 1981). This will be reported in detail in a coming paper by MOGI. The decrease in m-value under an applied constant stress means that the relative increase in the number of emission events with larger amplitude is not due directly to the increase in stress level itself. The effect can be explained reasonably if the stress drop and/or the source dimension (crack size) of emission events become larger in statistical terms as rock approaches failure. If the effect results entirely from the

relative change in size distribution of stress-induced cracks with time, then the effect will also be expressed in terms of frequency contained in emission waves because acoustic waves emitted from larger cracks will tend to contain lower frequency components.

In order to try to clarify these problems, we investigate in this paper frequency dependence of acoustic emission rate under incremental, uniaxial compression of rocks by taking an approach different from that of the earlier authors. A piezoelectric transducer in general has multiple sensitivity peaks (see next section). We utilize some of these peaks and accentuate them through the use of bandpass filters to set narrow bands of frequency windows through which to monitor acoustic emission, and compare the count rate of the emission events monitored through a low frequency window with that of those monitored simultaneously through a higher frequency window throughout an experimental run.

The characteristics of the monitoring system (including the sensor itself) are very important in investigating this kind of subject; however, few authors have included a detailed description of the systems used (HARDY, 1972). In addition, statistical approach is required so long as the spectra of acoustic emission are compared, because one emission event differs in the waveform and the frequency content from another, as will be shown later, and because a large number of such events are generated during a short time interval; say, several tens or more per second. Even if we deal with only the relatively large events above a certain level of threshold, it will not be possible to examine the spectra of the waves from all of these events. Hence, indispensable is statistical inference which is concerned with getting information from a sample of data about the population from which the sample is drawn. Such a statistical approach has been neglected in spite of its importance in most of the earlier studies, at least not reported in the literature, and the lack of a statistical approach makes these earlier studies less reliable. KUSUNOSE et al. (1980) took a statistical approach to investigate frequency dependence of acoustic waves under compressive stress, and argued that the spectral amplitudes at high frequencies become more dominant at higher stresses. It appeares, however, that their results are rather scattered to draw a definite conclusion.

In our approach, all of the emission events counted simultaneously through two different frequency windows under a fixed condition of the monitoring channels throughout a run are compared statistically. There is no methodological problem.

Experimental method

Figure 1 shows a block diagram of the monitoring system used, where overall frequency response of the amplification system is flat from 10 kHz to 2 MHz. The two receiving transducers, lead zirconate titanate disks polarized in the thickness direction each shielded by a metal case, were each attached to a specimen through a brass adapter, which was cemented to the side of the specimen with epoxy. The flat surfaces of both the transducers and the adapters used for monitoring higher frequency (>200 kHz) waves were carefully polished on plate glass with a finely powdered abrasive. Canada balsam was used as couplant between the polished contact-surfaces of both the transducers and the adapters to achieve good coupling. The transducers were fixed in place with the help of rubber bands.

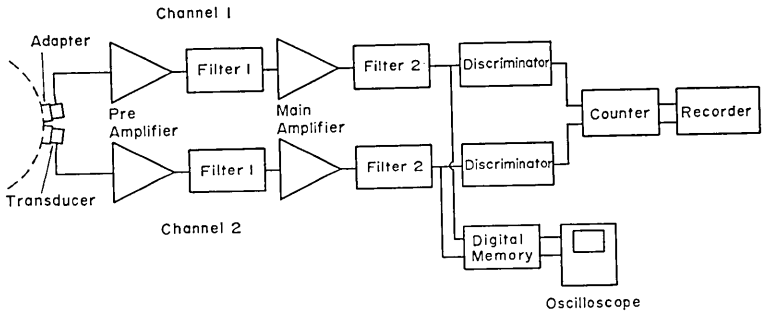

Fig. 1. Block diagram of overall acoustic emission monitoring system.

The output of each transducer was amplified and filtered, and the resulting signals were fed into an electronic circuitry which may be called discriminator, designed for assuring one pulse for one acoustic emission event by pertinently selecting both a threshold level of the comparator and a dead time of the gate. The pulses from the discriminator were counted by an electronic counter and, after converted to the analog signals and presented logarithmically, recorded by a strip-chart recorder to monitor the rate count of emission events during a test. In the present experiments the acoustic emission rate was sampled every 10 s for the duration of the tests. A dual-beam oscilloscope was used for checking the operation of the system and for monitoring the waveform of acoustic emission signals through a digital memory.

For such a transducer as a lead zirconate titanate disk polarized in the thickness direction, the electromechanical coupling factor is in general

of the same order of magnitude in the plane perpendicular to the polarization direction (namely, thickness direction) as in the polarization direction itself. For this reason, the piezoelectric transducer has sensitivity peaks at the frequencies resonant to each dimension of both thickness and diameter of the ceramic disk and to the dimension of the transducer case, and their higher modes will also appear. Hence, such a transducer cannot have a flat frequency response over a wideband of frequencies: it has multiple sensitivity peaks. Some of these peaks were utilized and accentuated through the use of active filters (bandpass) to set narrow bands of frequency-windows through which to monitor acoustic emission. Thus four different narrow bands of monitoring frequencies were selected for the present study; a low frequency window L (with sensitivity peaks around 30 kHz), two intermediate frequency windows I_1 ($\sim$250 kHz) and I_2 (250 kHz$\sim$400 kHz), and a high frequency window H ($\sim$1 MHz).

Figure 2 shows frequency responses of the overall monitoring channel for each frequency window selected above. These frequency responses were obtained by using nominally identical transducers (kept in contact with the two opposite faces of a metal disk) for both transmitting and receiving a sinusoidal wave over a wide range of frequencies, and by adjusting the gain of the amplifiers so as to have nearly the same sensitivity peaks between the monitoring channels for the four different frequency-windows selected. Since only two channels of the monitoring facilities were available for this study, two frequency windows such as (L, I_2) and (I_1, H) were chosen out of the four for an experiment and acoustic emission events were monitored and counted simultaneously through the two different frequency windows throughout the experimental run.

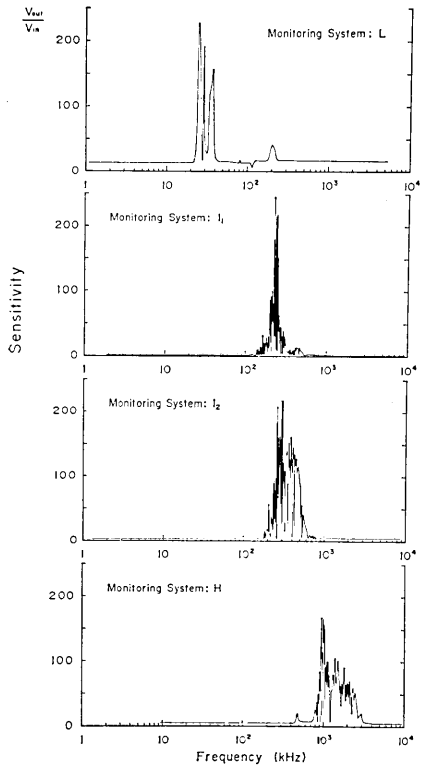

Fig. 2. Four different frequency windows selected and their overall frequency responses.

The duration time of acoustic waves varies according to a frequency window through which the acoustic waves are observed, as shown in

Figures 3 and 4. Preliminary experiments were made to check the duration time of acoustic waves generated during the fracturing process of rock specimens through each frequency window selected. By taking into consideration the observed values of the duration time of the acoustic waves through each frequency window, suitable values of the dead time for the gate of each channel were determined; about 2 ms for the low frequency window L, about 0.5 ms for the intermediate frequency windows I_1 and I_2, and about 0.04 ms for the high frequency window H. The threshold level of each channel was balanced pertinently above the noise level before each experiment so as to keep the count rates from the two different channels significant and comparable. If all the emission events above the noise level, including very small events, are taken into consideration, then some bursts of emission observed may be composed of several emission events occurring within the same time interval, making it impossible to assure one pulse for one emission event. To avoid such a situation, it is intended in this study that only the large acoustic events exceeding a certain, relatively high level of threshold far above the noise level be monitored and counted.

The rock samples selected for this study were of Shinkomatsu andesite and Mannari granite. The modal analysis, the porosity and the bulk density for these rocks are given in Table 1. The shape of the specimens used was right circular cylinder, 12.5 cm long and 5 cm in diameter, cored in the same direction from a single block. The ends were ground parallel. Steel end caps and epoxy fillets were affixed to the ends of the specimens in a manner similar to that described by MOGI (1966) to reduce end effects. SCHOLZ (1968b) showed that most of the emission events generated during compression for this kind of sample design are concentrated within

Table 1. Rocks studied.

Rock	Porosity (%)	Bulk density (g/cm^3)	Modal analysis (%)
Shinkomatsu andesite	5.3	2.47	phenocryst 31.6 plagioclase 28.8, augite 1.8, hypersthene 0.5, magnetite 0.5. groundmass 68.4 plagioclase 45.0, pyroxene 19.4, opaque mineral 4.0.
Mannari granite	0.7	2.62	quartz 31.1, plagioclase 23.9, K-feldspar 38.5, biotite 4.3, hornblende 0.3, opaque mineral 0.3, chlorite? 1.6.

the central section of the specimen rather than near the ends, as would be expected if stress concentrations owing to end effects were important. Electric resistance strain gages were directly cemented to the sample side surfaces both parallel and perpendicular to the cylinder axis to get volumetric strain.

Incremental loading experiments under uniaxial compression have been made on these specimens. Load was applied by a hydraulic testing apparatus until failure occurred. In each experiment two different transducers were used to monitor acoustic waves simultaneously through the two different frequency windows, as described above. These two transducers were put adjacent to each other to minimize the effect of propagation path, and both were put selectively either near the end or at the middle of a specimen to check the effect of transducer site on the emission count level.

Experimental results

Since an emission event is a rapid physical change in a material and acoustic emission is basically pulse transient in nature, the emission waves are in general thought to contain a broad spectrum of frequencies. It was found in practice, however, that one emission event differs from another in both the waveform observed and the frequency content. Some of these examples observed during the experiments are given in Figures 3 and 4. Figures 3(a_1) and (a_2) give examples of emission events which appeared simultaneously through the frequency windows I_1 and H, indicating that these events have both intermediate (~250 kHz) and high (~1 MHz) frequency wave components. Figures 3(b_1) and (b_2) show examples of the events which have dominant high frequency wave components, but few intermediate frequency components, while Figures 3(c_1) and (c_2) show examples of the events having dominant intermediate frequency waves, but few high frequency waves. It should be noted that these emission waves, different in both the amplitude and the frequency content, were observed despite the fact that the applied stress was held nearly constant. This is the reason why the statistical approach is indispensable when frequency dependence of acoustic emission is investigated by comparing the spectra. Figures 4(a), (b) and (c) show other examples of the emission waves different in the frequencies contained: an emission event having both low (~30 kHz) and higher (~250 kHz) frequency wave components (Figure 4(a)); an event having few low frequency components, but dominant higher frequency components (Figure 4(b)); an event having

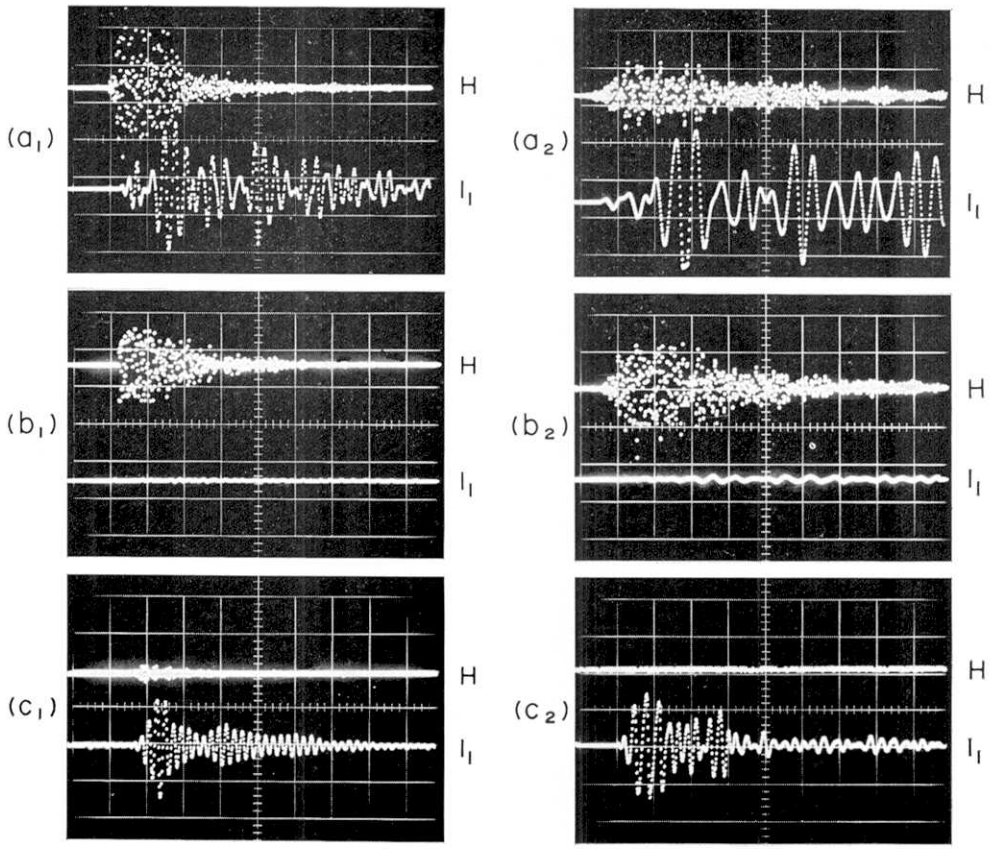

Fig. 3. Oscilloscope photographs of acoustic emission: comparison of the emission waves monitored through the high frequency window H with those monitored simultaneously through the intermediate frequency window I_1. (a_1) and (a_2), examples of the events having both high frequency and intermediate frequency wave components; (b_1) and (b_2), examples of the events having high frequency wave components, but few intermediate frequency components; (c_1) and (c_2), examples of the events having intermediate frequency wave components, but few high frequency components. Time scale, 1 division=0.02 ms for (a_1), (b_1), (c_1) and (c_2), and 1 division=0.01 ms for (a_2) and (b_2).

dominant low frequency components, but few higher components (Figure 4(c)).

Figure 5(a) shows a plot of a typical example of acoustic emission counts, $n(L)$ and $n(I_2)$, per 10 s against time during the whole process from application of loading to failure for incremental, uniaxial compression of Shinkomatsu andesite. In this experiment, the two monitoring channels were operated at a gain of 80 db and on a threshold level of 0.5V. In Figure 5(c) the applied axial stress and the strains (axial, circumferen-

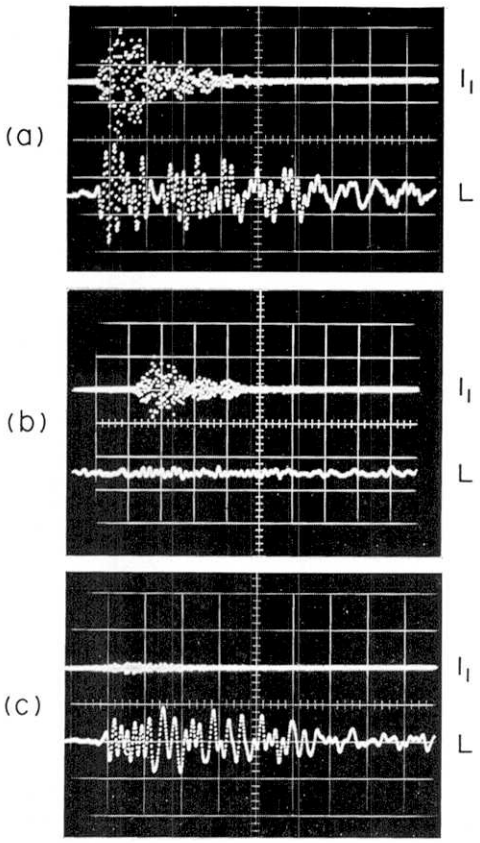

Fig. 4. Oscilloscope photographs of acoustic emission: comparison of the emission waves monitored through the intermediate frequency window I_1 with those monitored simultaneously through the low frequency window L. (a), an example of the events having both intermediate frequency and low frequency wave components; (b), an example of the events having intermediate frequency wave components, but few low frequency components; (c), an example of the events having low frequency wave components, but few intermediate frequency components. Time scale, 1 division =0.1 ms for (a), (b) and (c).

tial, and volumetric) are plotted against time for reference. As the axial compressive stress was increased, a flurry of acoustic emission activity occurred at low stresses, but this activity soon died down to a very low level. As the stress was further increased gradually, again acoustic emission activity began to build up and steadily increased, and then accelerated rapidly until failure. This pattern has been noticed by earlier authors (e. g., SCHOLZ, 1968a). In our experiments, a typical flurry of acoustic

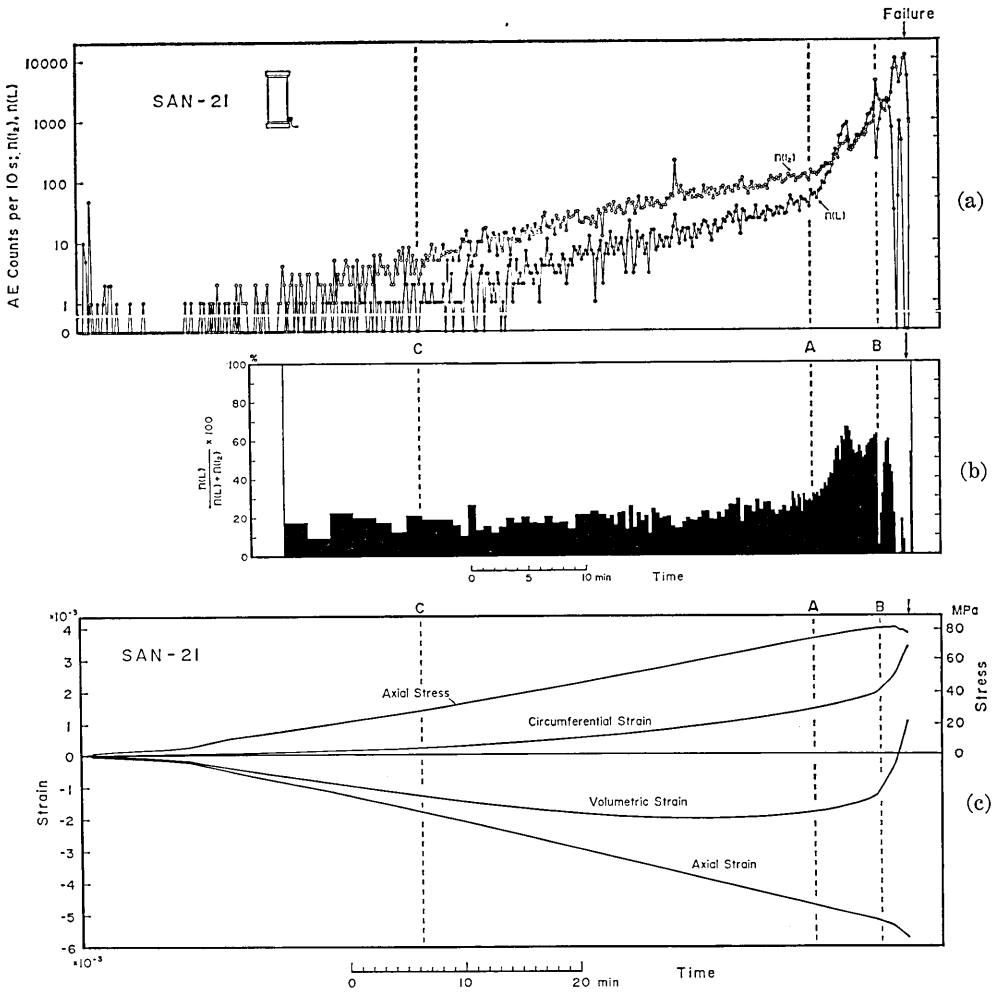

Fig. 5(a). A plot of acoustic emission counts per 10 s, $n(L)$ and $n(I_2)$ monitored through the low frequency window L and the intermediate frequency window I_2, respectively, against time during the whole process from application of loading to failure for incremental, uniaxial compression of Shinkomatsu andesite SAN-21. The inset shows the site where the transducers were attached.
(b). A plot of $n(L)/\{n(L)+n(I_2)\}$ against time for SAN-21.
(c). A plot of axial stress and strains (axial, circumferential and volumetric) against time for SAN-21.
The mark A indicates the point of time when $n(L)/\{n(L)+n(I_2)\}$ begins to increase with time; the mark B indicates the point of time at which a rapid acceleration of higher frequency acoustic emission rate begins; the point of time marked C corresponds to the upper limit of the linear portion of the stress-strain curve.

emission activity at low stresses was observed when acoustic emission was monitored through the low frequency window L. This is obvious from Figures 5 and 8, suggesting that almost all of the activity at low

stresses are due to the occurrence of such low frequency emission events as monitored only through the frequency window L.

We focus attention on frequency dependence of emission counts in the region where acoustic emission activity begins to build up and continues to increase until failure. We find from Figure 5(a) that at first $n(L)$ and $n(I_2)$ increase exponentially with time, keeping the ratio of $n(L)$ to $n(I_2)$ statistically constant [note that the ordinate of Figure 5(a) is on a logarithmic scale]. Thereafter, as seen in Figure 5(a), both $n(L)$ and $n(I_2)$ increase supraexponentially with time: the increase rate of $n(L)$ is more rapid than that of $n(I_2)$. This tendency was followed by a very rapid rise in $n(I_2)$. In this experiment the count level of $n(L)$ was fairly lower than that of $n(I_2)$ until approximately 7 minutes before failure. Although it is apparent from Figure 5(a) that the increase rate of $n(L)$ becomes more rapid with time than that of $n(I_2)$, this is seen more clearly in Figure 5(b), where $[n(L)/\{n(L)+n(I_2)\}]\times 100$ is taken on the ordinate [note that $0<n(L)/\{n(L)+n(I_2)\}<1$ for any positive value of $n(L)$ and $n(I_2)$]. It is true that the count level itself depends upon the sensitivity and the threshold level set for each channel. But the threshold level and sensitivity were fixed throughout the experiment for each channel. Accordingly, the ratio $n(L)/\{n(L)+n(I_2)\}$ is a significant and useful parameter for checking frequency dependence of the emission rate. The change in the ratio defined above can be regarded as a measure of representing the frequency dependence of acoustic emission rate quantitatively.

Figure 5(b) suggests that the whole time process shown in the figure may be tentatively divided into two stages; an early stage where $n(L)/\{n(L)+n(I_2)\}$ is nearly constant, and a later stage which is characterized by an increase in $n(L)/\{n(L)+n(I_2)\}$ with time or by a higher level of $n(L)/\{n(L)+n(I_2)\}$. This could be an important generalization if it is universally true for any rocks, for any frequency ranges to be compared, and for any experimental conditions to be considered. In this experiment, the transducers were put near the end of the specimen, as shown in the inset. Formation of open axial cracks within rock under uniaxial compression has been verified by direct observation (TAPPONNIER and BRACE, 1976; KRANZ, 1979). Hence, one may argue for instance that the different site to which the transducers were attached might result in a different result from that shown in Figure 5, owing to anisotropic attenuation caused by formation of open axial cracks within a deforming rock specimen. To check this, experiments were repeated under the same monitoring conditions except for the site to which the transducers were attached: the transducers were put at the middle of specimens of the Shinkomatsu

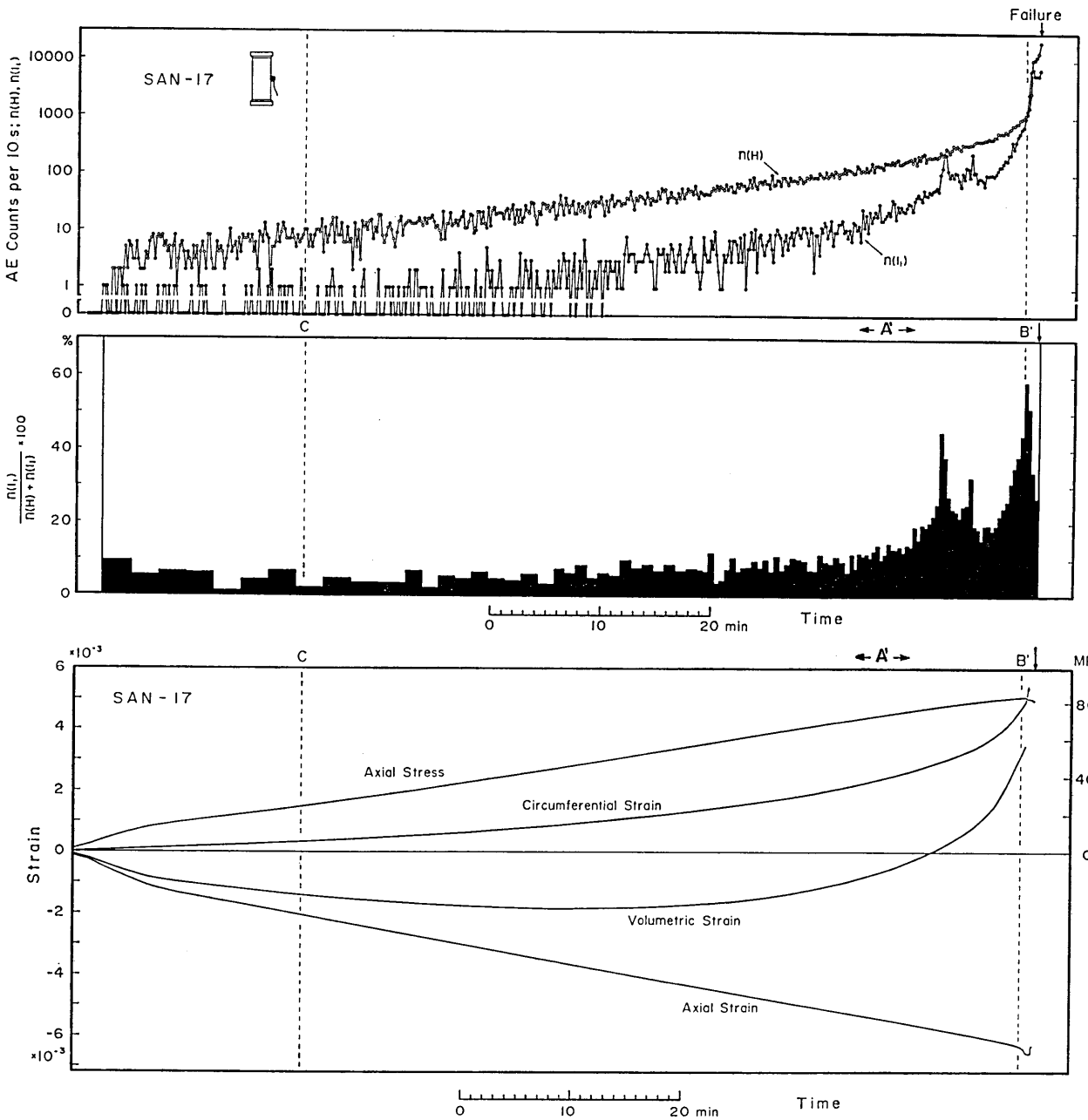

Fig. 6(a). A plot of acoustic emission counts per 10 s, $n(I_1)$ and $n(H)$ monitored through the intermediate frequency window I_1 and the high frequency window H, respectively, against time for incremental, uniaxial compression of Shinkomatsu andesite SAN-17. The inset shows the site where the transducers were attached.
(b). A plot of $n(I_1)/\{n(I_1)+n(H)\}$ against time for SAN-17.
(c). A plot of axial stress and strains (axial, circumferential and volumetric) against time for SAN-17.
The mark A′ indicates the point of time at which $n(I_1)/\{n(I_1)+n(H)\}$ begins to increase with time; the mark B′ indicates the point of time at which a very rapid acceleration of high frequency acoustic emission rate begins; the point of time marked C corresponds to the upper limit of the linear portion of the stress-strain curve.

andesite. These gave the same result as shown in Figure 5; the two stages defined above were distinctly found.

Further experiments have been made using the same rock to examine whether the relation obtained above holds true for the emission counts monitored simultaneously through different bands of higher frequencies. Figure 6(a) shows a plot of the event counts per 10 s, $n(I_1)$ and $n(H)$, through the frequency windows I_1 and H, respectively, against time. This is typical of these data. The inset shows the site where the transducers were attached. In Figure 6(b) the parameter $n(I_1)/\{n(I_1)+n(H)\}$ is plotted against time. Figure 6(c) shows a plot of the applied axial stress and of the strains (axial, circumferential and volumetric) against time on the same time scale. We find again that both $n(I_1)$ and $n(H)$ increase exponentially at first, and that thereafter there are supraexponential rises in both $n(I_1)$ and $n(H)$: in this stage the increase rate of $n(I_1)$ is more rapid than that of $n(H)$ until shortly before failure. Figure 7 shows another example of a plot of $n(I_1)$ and $n(H)$ versus time for incremental, uniaxial compression of Shinkomatsu andesite. The only difference of the experimental conditions between the results shown in Figures 6 and 7 was in the site where the transducers were attached, as shown in the insets. In both experiments the monitoring channel of H was operated at a gain of 80 db and on a threshold level of 0.3 V and the channel of I_1 was operated at a gain of 60 db and on a threshold level of 0.3 V. Note that the same effect was detected regardless of the difference in the site to which the transducers were attached. Thus, it is distinctly concluded that as the andesite rock approaches failure, the acoustic emission rate generated during the deformation, monitored through a low frequency window, increases more rapidly than that monitored simultaneously through a higher frequency window regardless of the difference in both the frequency bands compared and the site to which the transducers were attached.

In Figure 8, the acoustic event counts per 40 s, $n(L)$ and $n(I_2)$, are plotted against time for incremental, uniaxial compression of Mannari granite, and the applied axial stress and the strains (axial, circumferential and volumetric) of the specimen are also plotted against time for reference. In this experiment, the two monitoring channels were operated at a gain of 80 db and on a threshold level of 0.5 V. A typical flurry of acoustic emission activity at low stresses was observed. We notice from Figure 8(a) that until about 20 minutes after application of loading the count level of $n(L)$ was higher than that of $n(I_2)$, and that thereafter the count level of $n(I_2)$ then became higher than that of $n(L)$. The count levels

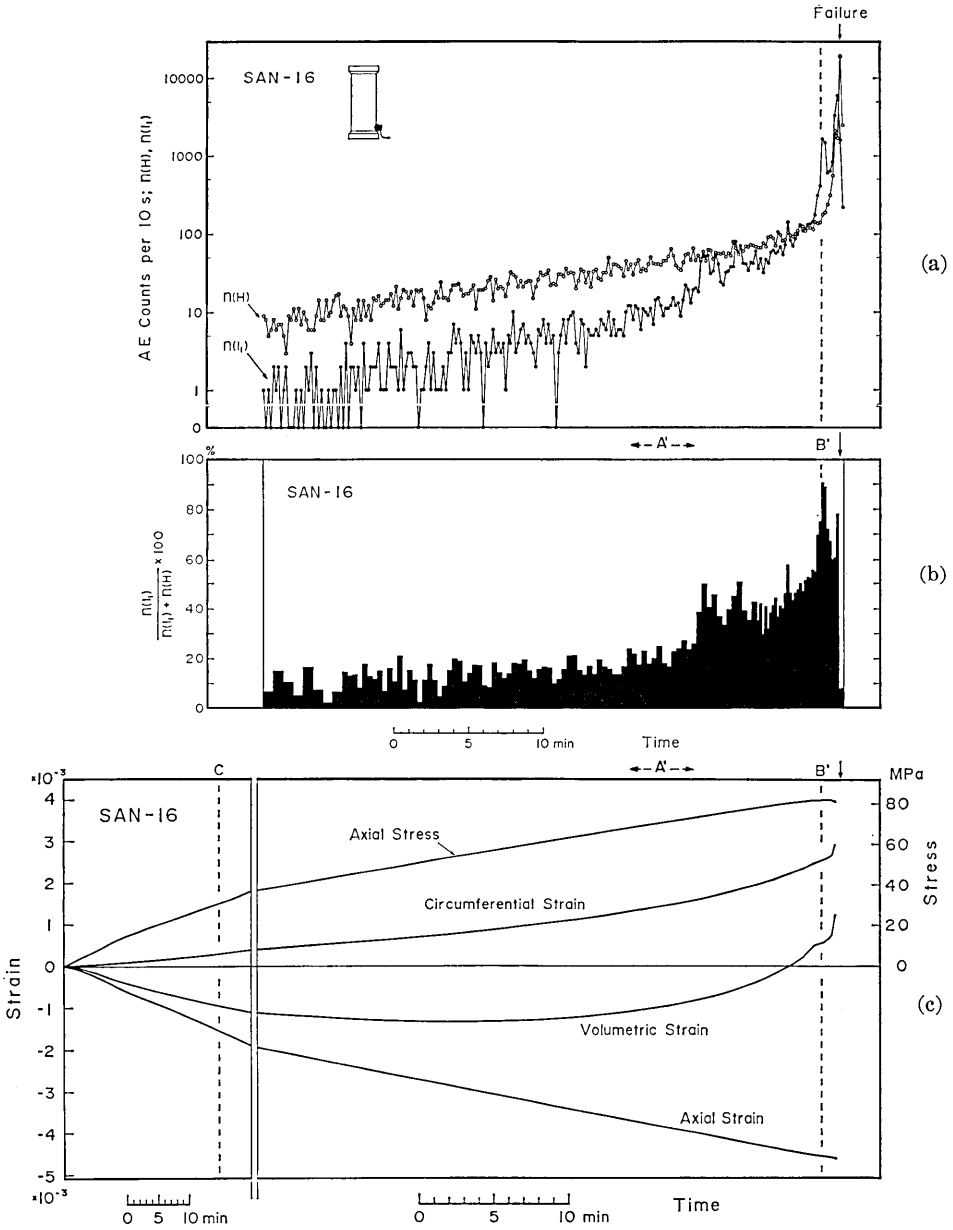

Fig. 7(a). A plot of acoustic emission counts per 10 s, $n(I_1)$ and $n(H)$ monitored through the intermediate frequency window I_1 and the high frequency window H, respectively, against time for incremental, uniaxial compression of Shinkomatsu andesite SAN-16. The inset shows the site where the transducers were attached.
(b). A plot of $n(I_1)/\{n(I_1)+n(H)\}$ against time for SAN-16.
(c). A plot of axial stress and strains (axial, circumferential and volumetric) against time for SAN-16.
For explanations of the points marked A′, B′ and C see the caption of Figure 6.

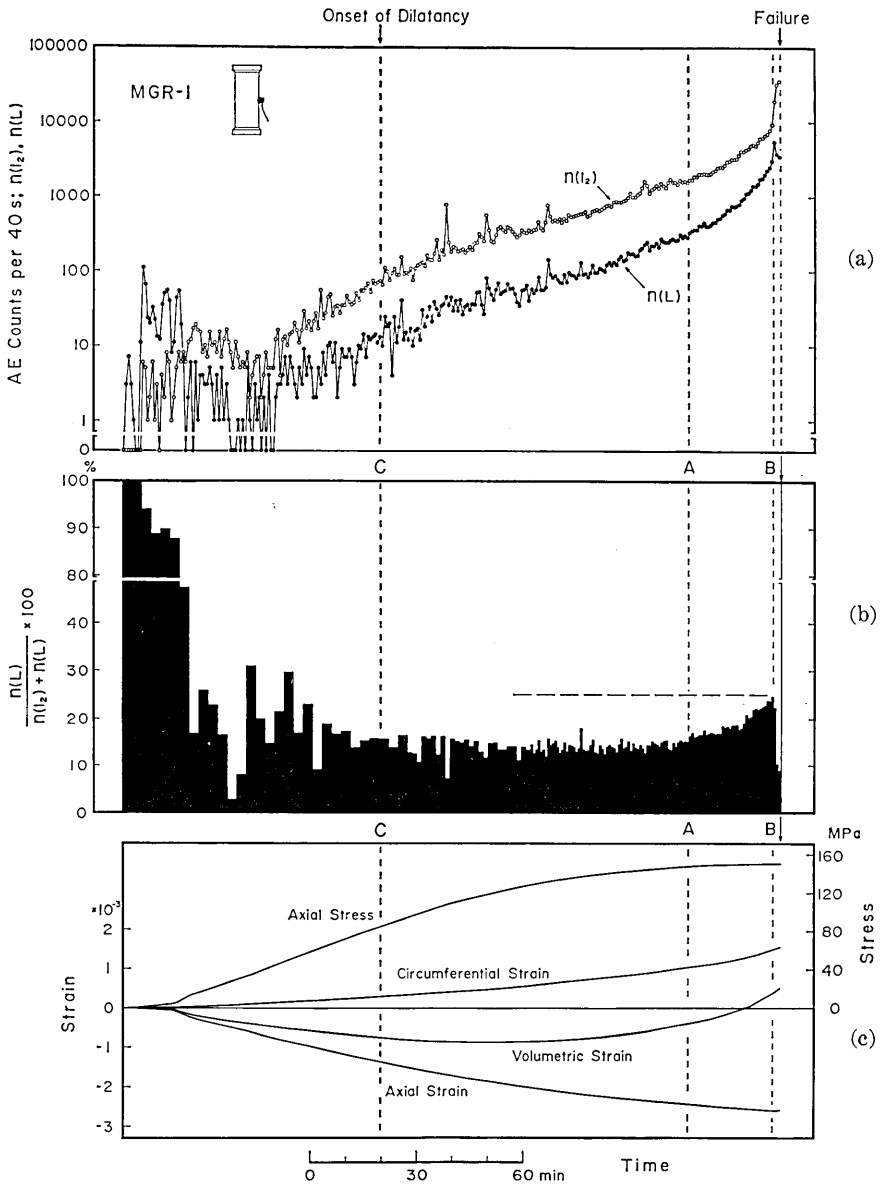

Fig. 8(a). A plot of acoustic emission counts per 40 s, $n(L)$ and $n(I_2)$ monitored through the low frequency window L and the intermediate frequency window I_2, respectively, against time during the whole process from application of loading to failure for uniaxial compression of Mannari granite MGR-1. The inset shows where the transducers were attached.

(b). A plot of $n(L)/\{n(L)+n(I_2)\}$ against time for MGR-1.

(c). A plot of axial stress and strains (axial, circumferential and volumetric) against time for MGR-1.

The mark A indicates the point of time at which $n(L)/\{n(L)+n(I_2)\}$ begins to increase with time; the mark B indicates the point of time at which a rapid acceleration of higher frequency acoustic emission rate begins; the mark C indicates the point of time at which appreciable dilatancy begins.

differed considerably between $n(L)$ and $n(I_2)$. We find also from Figure 8 that as the failure time approaches the increase in both $n(L)$ and $n(I_2)$ becomes supraexponential with time, and that the increase rate of $n(L)$ is more rapid until a few minutes before failure than that of $n(I_2)$. Failure occurred shortly after $n(L)/\{n(L)+n(I_2)\}$ lowered. These qualitative features are entirely consistent with those found for Shinkomatsu andesite, though the parameter $n(L)/\{n(L)+n(I_2)\}$ varied to a lesser extent with time near failure for Mannari granite than for Shinkomatsu andesite. Further experiments were performed to examine whether the same effect is detected for the emission events monitored through the higher frequency windows I_2 and H for incremental compression of Mannari granite. These confirmed the foregoing results.

Figure 8 suggests that after a flurry of acoustic emisson activity at low stresses, the emission rate increases exponentially only when the stress rate is constant. Note that there is a correlation between the slopes of the emission counts-time curve and of the applied stress-time curve in the early stage.

One may argue that the frequency dependence of acoustic emission rate described above is due directly to the increase in an applied stress level. It is clear, however, that this frequency dependence is not a direct result of the variation in an applied stress level. In the experiment of which result is shown in Figure 8, the loading rate was held approximately constant until nearly the half of the whole time from application of loading to failure, and then it was gradually decreased to zero. Hence, the applied stress was held nearly constant near failure [see Figure 8(c)]. Nevertheless, the increase rate of acoustic emission counts monitored through a low frequency window became more rapid with time until shortly before failure than that of the counts monitored simultaneously through a higher frequency window as the failure time approached. This means that the frequency dependence of acoustic emission rate is not necessarily caused by the change in an applied stress level. We suggest that the frequency dependence should be attributed to the change in structural state within a deforming rock specimen under compression. This will be discussed in more detail in next section.

Discussion

SCHOLZ (1968a) pointed out that the pattern of acoustic emission activity during deformation of brittle rock under incremental compression is closely related to the stress-strain behavior. At low stresses in

the region in which a flurry of acoustic emission activity occurs, the stress-strain curve is nonlinear. At higher stresses where acoustic emission activity is very low, the rock deforms elastically, and the resumption of acoustic emission corresponds to the beginning of nonlinearity of the upperpart of the stress-strain curve. The nonlinear part of the stress-strain curve above about half the failure strength is the region where dilatancy occurs (BRACE et al., 1966). Dilatancy in this stage is directly proportional to acoustic emission activity (SCHOLZ, 1968a).

However, if examined in more detail, it generally seems inaccurate to characterize acoustic emission activity as such in relation to the stress-strain curve; for example, the beginning of a sequence of acoustic emission activity does not necessarily correspond to the onset of dilatancy which is defined as the beginning of the nonlinear part of the stress-strain curve above about half the failure strength. In general, if the sensitivity of the monitoring system is high, the beginning of a sequence of acoustic emission activity can be observed at lower stresses. In the present experiments, the sequence of acoustic emission activity in practice began at low stresses where appreciable dilatancy cannot occur [see Figures 5, 6, and 8, where the point of time marked C corresponds to the upper limit of the linear portion of the stress-strain curve. This is the point at which dilatancy begins for a low porosity rock such as granite. For Shinkomatsu andesite having high porosity, however, actual dilatancy may accurately not begin at that point for the reason stated below; the point of time marked C only suggests the approximate onset of dilatancy for the rock].

In particular for high porosity rocks such as Shinkomatsu andesite, the closing of pores, the resulting compaction and the induced microcracks can occur at the same time during the deformation process from application of loading to failure. As a result the effect of compaction and dilatancy becomes more difficult to separate. BRACE (1978) has pointed out that both compaction and dilatancy occur at the same time when rocks have more than about 5% porosity. For this reason, the actual onset of dilatancy is less easily identified in these rocks, and hence it is more difficult to relate acoustic emission activity during the deformation to dilatancy itself for these rocks than for low porosity rocks.

We pointed out in the previous section that a flurry of acoustic emission activity at low stresses is due to the occurrence of the emission events monitored only through the low frequency window L. One may argue that such a flurry of the activity at very low stresses may be noises caused by the adjustment (or friction) of a spherical seat used as

loading axis adjuster. This possibility must be considered and may not entirely be rejected. However, the existence of pre-existing cracks with such low aspect ratio as 10^{-3} in rock (SPRUNT and BRACE, 1974; KRANZ, 1979) also strongly suggests that the closing of such pre-existing cracks at large angles to the compression axis at very low stresses results in the generation of low frequency acoustic waves.

Previously we tentatively divided the region where a sequence of acoustic emission activity occurs and continues to increase into the two distinct stages on the basis of the result shown in Figure 5 for Shin-komatsu andesite. This will be more generally described if all the results shown in the previous section are considered. The deformation process of brittle rock under incremental compression may be commonly divided into the following five stages in terms of the acoustic emission rates. At low stresses in the region where a flurry of acoustic emission activity occurs, the activity is mostly due to low frequency acoustic emissions, presumably resulting from the closing or the shearing of pre-existing cracks with low aspect ratio (first stage). At higher stresses the activity dies down to a very low level (second stage). As the stress is further increased gradually, again acoustic emission activity begins to build up and steadily increases [the emission rate increases exponentially when the loading rate is held constant]. Both the emission rates $n(l)$ and $n(h)$ monitored through a low frequency window and a higher frequency window, respectively, increase with time at statistically the same proportion; that is, $n(l)/\{n(l)+n(h)\}$ is nearly constant throughout this stage (third stage). As the failure time is approached, both $n(l)$ and $n(h)$ increase supraexponentially with time, and the increase rate of $n(l)$ becomes more rapid than that of $n(h)$ until immediately before failure (fourth stage: from the point of time marked A or A′ to the point of time marked B or B′ in Figures 5 to 8). In other words, this stage is characterized by an increase in $n(l)/\{n(l)+n(h)\}$ with time or by a higher level of $n(l)/\{n(l)+n(h)\}$. The fifth (final) stage (from the point of time marked B or B′ to the failure time in Figures 5 to 8) is characterized by a very rapid acceleration of $n(h)$ immediately before and during failure. As a result, failure occurs immediately after $n(l)/\{n(l)+n(h)\}$ is lowered.

One interesting feature in these stages is that the increase rate of the acoustic emission counted through a lower frequency window becomes more rapid with time in the fourth stage. This is not necessarily due to the change in an applied stress level itself, as described in the previous section, but due to the change in microstructure within a deforming rock specimen. There are two possible explanations for this:

1) As an applied load increases, microfractures will occur and the resulting microcracks will further grow to some extent and develop (or coalesce) in the course of deformation. Opening or shearing of these existing cracks into larger sizes will tend to generate emission waves including lower frequency components. The number of these larger cracks is likely to increase greatly with time as rock approaches failure. As a result lower frequency emission waves will be more acceleratedly generated in this stage, and

2) As an applied load increases, microcracks will increase in number and will be distributed within a rock specimen during the deformation, causing a dilatant region within it. The development of such a dilatant region has the effect of attenuating emission waves. In a stage where dilatancy is pronouncedly and widely developed, the emission events with low frequency wave components become more highly detectable. Higher frequency wave components are more highly attenuated as they propagate away from the sources. This will contribute to explaining the present observation if attenuation increases as rock approaches failure.

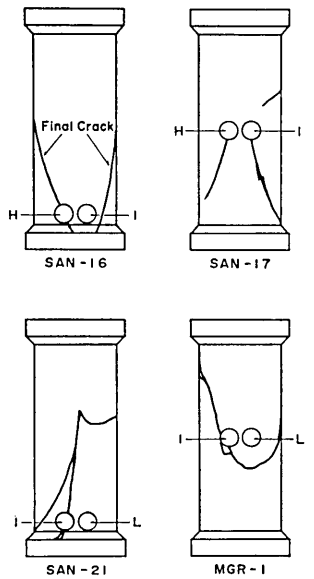

Fig. 9. Relations between the site to which the transducers were attached and the final macroscopic crack pattern. L, transducer site used for monitoring low frequency emission waves; I, transducer site for intermediate frequency emission waves; H, transducer site for high frequency emission waves. The thick lines represent the location of macroscopic fracture surfaces which were observed when the specimens eventually failed.

Presumably both explanations are partly responsible for the observed frequency dependence; however, it is difficult to determine from the present experiments to what extent each is responsible. It should be emphasized here that the beginning of the fourth stage is not concurrent with the onset of dilatancy. Appreciable dilatancy always begins to occur prior to the beginning of the fourth stage (see Figure 8).

A greater number of higher frequency emission events observed in the final stage may be thought to be those originating around the transducers as a result of local stress concentrations near the adapters during the process of forming final faults. Figure 9 shows the relation between the sites to which the transducers were attached and the final macro-

scopic crack pattern for each test specimen. The thick lines represent the location of macroscopic fracture surfaces which were observed when the specimens eventually failed. The crack patterns in the figure in fact suggest that the transducer sites are sources of stress concentration.

We have found in this series of experiments that the acoustic emission rate $n(l)$ monitored through a low frequency window increases more rapidly than the emission rate $n(h)$ monitored through a higher frequency window as rock approaches failure under compression, and that failure occurs shortly after $n(l)/\{n(l)+n(h)\}$ is lowered. This effect may be used for understanding structural instability of the region where earthquakes can occur potentially, and consequently for predicting the time when a main earthquake occurs in the region, in terms of frequency contained in seismic waves if a sizable microearthquake population is observed through transducers placed near the fault.

In the statistical analysis of acoustic emission in the fracturing process of rock, a common way of displaying the amplitude distribution data is to use a log-log plot of the cumulative number of events versus the maximum trace amplitude, as was described in the Introduction section. The slope of the curve which is a manifestation of the amplitude distribution is called "m-value" or "b-value". It has been reported that the m-value decreases as rock approaches failure. The decrease in m-value means that the number of emission events with larger amplitude increases more greatly in relative terms as rock approaches failure. SCHOLZ (1968c) observed the decrease in m-value under the incremental compressive stress, and he ascribed the decrease in m-value to the increase in the stress level. MOGI (1981), however, carried out careful experiments under a constant stress and still found an appreciable decrease in m-value before failure. This shows that the relative increase in the number of emission events with larger amplitude is not a direct result of the increase in stress level itself. The effect can be explained reasonably if the stress drop and/or the source dimension (crack size) of emission events become larger in statistical terms as rock approaches failure. If the effect is a manifestation of the fact that the number of crackings resulting in larger size increases more in relative terms as rock approaches failure, the decrease in m-value is consistent with the frequency dependence of acoustic emission rate found in the present experiments (fourth stage). Crackings resulting in larger size tend to generate acoustic waves with both larger amplitudes and lower frequency components. Presumably, the decrease in m-value and the frequency dependence of acoustic emission rate are different manifestations of an aspect of the fracturing process to failure

of brittle rock.

It is possible to discuss the microfracturing process to failure of brittle rock in more detail on the basis of the present results. This will be done in another paper (OHNAKA and MOGI, 1981).

References

BRACE, W.F., 1978, Volume changes during fracture and frictional sliding: a review, *Pageoph*, **116**, 603-614.

BRACE, W.F., PAULDING, B.W., Jr. and SCHOLZ, C., 1966, Dilatancy in the fracture of crystalline rocks, *J. Geophys. Res.*, **71**, 3939-3953.

BYERLEE, J., 1978, A review of rock mechanics studies in the United States pertinent to earthquake prediction, *Pageoph*, **116**, 586-602.

CHUGH, Y.P., HARDY, H.R., Jr. and STEFANKO, R., 1968, An investigation of the frequency spectra of microseismic activity in rock under tension, Presented at the Tenth Rock Mech. Sym., Austin, Texas, May.

FEDOTOV, S.A., GUSEV, A.A. and BOLDYREV, S.A., 1972, Progress of earthquake prediction in Kamchatka, *Tectonophysics*, **14**, 279-286.

HARDY, H.R., Jr., 1972, Application of acoustic emission techniques to rock mechanics research, *Acoustic Emission, ASTM STP 505*, Amer. Soc. Test. Materials, 41-83.

HARDY, H.R., Jr., 1977, Emergence of acoustic emission, microseismic activity as a tool in geomechanics, *Proc. First Conf. Acoustic Emission/Microseismic Activity in Geologic Structures and Materials*, Trans. Tech. Publications, 13-31.

KANAGAWA, T., HAYASHI, M. and NAKASA, H., 1977, Estimation of spacial geo-stress components in rock samples using the Kaiser effect of acoustic emission, *Proc. Japan Soc. Civ. Engi.*, No. 258, 63-75 (in Japanese).

KNILL, J.L., FRANKLIN, J.A. and MALONE, A.W., 1968, A study of acoustic emission from stressed rock, *Int. J. Rock Mech. Min. Sci.*, **5**, 87-121.

KRANZ, R.L., 1979, Crack growth and development during creep of Barre granite, *Int. J. Rock Mech. Min. Sci. & Geomech. Abstr.*, **16**, 23-35.

KUSUNOSE, K., YAMAMOTO, K. and HIRASAWA, T., 1980, Source process of microfracture in granite with reference to earthquake prediction, *Sci. Rep. Tohoku Univ. Ser. 5, Geophysics*, **26**, 111-121.

MOGI, K., 1962a, Study of elastic shocks caused by the fracture of heterogeneous materials and its relations to earthquake phenomena, *Bull. Earthq. Res. Inst., Tokyo Univ.*, **40**, 125-173.

MOGI, K., 1962b, Magnitude-frequency relation for elastic shocks accompanying fractures of various materials and some related problems in earthquakes, 2, *Bull. Earthq. Res. Inst., Tokyo Univ.*, **40**, 831-853.

MOGI, K., 1966, Some precise measurements of fracture strength of rocks under uniform compressive stress, *Felsmech. Ingenieurgeol.*, **4**, 41-55.

MOGI, K., 1967, Earthquakes and fractures, *Tectonophysics*, **5**, 35-55.

MOGI, K., 1973, Rock fracture, *Ann. Rev. Earth Planet. Sci.*, **1**, 63-84.

MOGI, K., 1981, Earthquake prediction in Japan, *Marice Ewing Series 3* (in press).

OBERT, L., 1941, Use of subaudible noise for prediction of rock bursts, *U.S. Bureau of Mines Rept. Invest.* 3555.

OBERT, L. and DUVALL, W.I., 1942, Use of subaudible noise for prediction of rock bursts—Part II, *U.S. Bureau of Mines Rept. Invest.* 3654.

OHNAKA, M. and MOGI, K., 1981, Frequency characteristics of acoustic emission in rocks under compression and its relation to the fracturing process to failure, Sub-

mitted to *J. Geophys. Res.*

SCHOLZ, C. H., 1968a, Microfracturing and the inelastic deformation of rock in compression, *J. Geophys. Res.*, **73**, 1417-1432.

SCHOLZ, C. H., 1968b, Experimental study of the fracturing process in brittle rock, *J. Geophys. Res.*, **73**, 1447-1453.

SCHOLZ, C. H., 1968c, The frequency-magnitude relation of microfracturing in rock and its relation to earthquakes, *Bull. Seis. Soc. Amer.*, 58, 399-415.

SHAMINA, O. G., 1956, Elastic pulses in the fracture of rock samples, *Bull. (Izv.) Acad. Sci. USSR, Geophysics Ser.* No. 5, 513-518 (in Russian).

SHAMINA, O. G., 1975, Modeling of earthquakes, *Izv., Earth Phys.*, No. 10, 10-20.

SPRUNT, E. S. and BRACE, W. F., 1974, Direct observation of microcavities in crystalline rocks. *Int. J. Rock Mech. Min. Sci. & Geomech. Abstr.*, **11**, 139-150.

TAPPONNIER, P. and BRACE, W. F., 1976, Development of stress-induced microcracks in Westerly granite, *Int. J. Rock Mech. Min. Sci & Geomech. Abstr.*, **13**, 103-112.

UTSU, T., 1980, Spatial and temporal distribution of low-frequency earthquakes in Japan, *J. Phys. Earth*, 28, 361-384.

4. 一軸圧縮増加応力下における岩石のアコースティック・エミッション発生頻度の周波数依存性

地震研究所 大中康譽・茂木清夫

常温・一軸圧縮応力下における岩石の変形過程で発生するアコースティック・エミッション（AE）の頻度に周波数依存性がみられるかどうか，もしみられるとすれば試料内部の微小破壊の進行と共にどう変化するかを実験的に詳細に調べた．

一般に，PZT のような圧電素子では分極軸に直交する方向でも電気機械結合係数が分極方向と実際には同程度故，厚み，直径（円板状の場合）の両サイズに対応した共振周波数でそれぞれ大きな感度を持つ．同時にそれらの高調波もあらわれる．さらに，この圧電素子を金属容器に固定して換振器とすると容器との結合による共振が別にあらわれる．したがって，このような換振器の周波数特性は一般に極めて複雑で広範囲にわたり感度差が著しい．筆者らは，圧電素子による換振器のこのような特徴をむしろ積極的に利用することにし，特定の周波数付近のピークを残し，他はすべてフィルターで消すことによって，限られた周波数範囲の窓 L (~30 kHz)，I_1 (~250 kHz)，I_2 (250 kHz~400 kHz)，H (~1 MHz) を用意し，実験毎に各窓を通じて得られる AE イベントの発生率を加荷重開始点から破損に至る全過程を通じて計数した。イベント計数法ではデッドタイム及びしきい値の設定を的確にしなければならない．各周波数窓から得られる AE 波形の継続時間は異なる故，予備実験により多数の AE 波形を観測し，適当なデッドタイムを各周波数の窓毎に定めた．しきい値が低いと，AE 最頻発時には波形が互いに重なり合い見かけ上一連の波形となって，イベントの識別が不可能になる。これを避けるため，しきい値をノイズレベルよりはるかに高く設定した．AE は1イベント毎に波形（振幅，周波数）が異なる故，周波数依存性を調べるためには統計的処理が不可欠である．本方法のユニークな点は，破損までの全過程を通じチャンネル毎に一定の条件を満たすイベント全てを計数するので，チャンネル間の統計的比較が容易にできることである．試料として直径 50 mm，高さ 125 mm の円柱状に整形された新小松安山岩，万成花崗岩を用い，換振器を試料側面の中央部又は端部に固定した．

本研究によって，岩石の破損近傍で AE 発生率の顕著な周波数依存性が見い出された．この周波数依存性および AE 発生率の特徴によって，加荷重から破損までの全過程は次の5段階に分けられるようである：I，低応力下における低周波数 AE 活動卓越期．II，AE 活動静穏期．III，応力増大と共に AE 活動が増大（荷重速度一定なら AE 発生率は指数関数的に増加）し，かつ低周波数 AE，高周波数 AE 発生比率のほぼ一定な段階．IV，AE 発生率が超指数関数的に増大しかつ高周波数 AE 発生率に比し低周波数 AE 発生率のより増大する段階．V，主破壊の急激な進行及び直前における高周波数イベント発生率の急増の最終段階．第 IV 段階の低周波数イベント計数率の増大に対しては2つの可能な説明が考えられる．すなわち，破損が近づくにつれて，大クラックがより多数形成されること，および高周波数弾性波の減衰がより顕著になることである．このどちらも低周波数イベント計数率の増大に寄与する．このことは，大振幅波形を持つイベント数が破損前に相対的に増大する事実（振幅別累積度数分布を両対数で表示したときの傾き m の減少）と調和する。第 IV 段階でみられる AE の周波数依存性と m 値の減少とは岩石の微視的破壊過程における同一事象の異なった表現と見ることができるであろう．最終段階における高周波数イベント数の急増は，主破壊の急激な進行に関連して換振器近傍に発生した高周波数イベント数の増大を示すと思われる．